Physics in Medicine & Biology





OPEN ACCESS

RECEIVED

19 November 2024

REVISED

28 January 2025

ACCEPTED FOR PUBLICATION 20 February 2025

PUBLISHED

3 March 2025

Original content from this work may be used under the terms of the Creative Commons Attribution 4.0 licence.

Any further distribution of this work must maintain attribution to the author(s) and the title of the work, journal citation and DOI.



PAPER

Evaluation of motion mitigation strategies for carbon ion therapy of abdominal tumors based on non-periodic imaging data

Timo Steinsberger^{1,10}, Anestis Nakas^{2,10,*}, Alessandro Vai⁵, Silvia Molinelli⁵, Marco Donetti⁸, Marco Pullia⁸, Maria Chiara Martire^{1,4}, Cosimo Galeone^{1,4}, Mario Ciocca⁵, Andrea Pella⁷, Viviana Vitolo⁶, Amelia Barcellini^{6,9}, Ester Orlandi⁶, Sara Imparato⁶, Lennart Volz¹, Guido Baroni^{2,7}, Chiara Paganelli², Marco Durante^{1,3} and Christian Graeff^{1,4}

- GSI Helmholtzzentrum für Schwerionenforschung GmbH, Biophysics, Darmstadt, Germany
- Politecnico di Milano, Department of Electronics, Information and Bioengineering, Milano, Italy
- Technical University of Darmstadt, Institute of Condensed Matter Physics, Darmstadt, Germany
- Department of Electrical Engineering and Information Technology, Technical University of Darmstadt, Darmstadt, Germany
- ⁵ Department of Medical Physics, CNAO National Center for Oncological Hadrontherapy, Pavia, Italy
- ⁶ Clinical Department, CNAO National Center for Oncological Hadrontherapy, Pavia, Italy
- ⁷ CNAO National Center for Oncological Hadrontherapy, Bioengineering Unit, Pavia, Italy
- Research Department, CNAO National Center for Oncological Hadrontherapy, Pavia, Italy
- ⁹ Department of Internal Medicine and Therapeutics, University of Pavia, Pavia, Italy
- ¹⁰ Both authors share first authorship.
- * Author to whom any correspondence should be addressed.

E-mail: anestis.nakas@polimi.it

Keywords: carbon-ion radiotherapy, motion mitigation, time-resolved MRI, 4DMRI

Abstract

Objective. To identify suitable combination strategies for treatment planning and beam delivery in scanned carbon ion therapy of moving tumors. Approach. Carbon ion treatment plans for five abdominal tumors were optimized on four-dimensional (4D) computed tomography (CT) data using the following approaches. 4DITV across all phases and within a gating window, single phase uniform dose, and an innovative 4D tracking internal target volume (ITV) strategy. Delivered single-fraction doses were calculated on time-resolved virtual CT images reconstructed from 2D cine-magnetic resonance imaging series, using a deformable image registration pipeline. Treatment plans were combined with various beam delivery techniques: three-dimensional (no motion mitigation), rescanning, gating, beam tracking, and multi-phase 4D delivery with and without residual tracking (MP4D and MP4DRT) to form in total 11 treatment modalities. Single fraction doses were accumulated to simulate a fractionated treatment. Main results. Breath-sampled treatments using the MP4D and MP4DRT delivery techniques were the only to achieve $D_{95} > 95\%$ for hypofractionated treatments, with little dependence on the number of fractions. A combination of MP4DRT with the new 4D tracking ITV approach resulting in conformal dose distributions and demonstrated the greatest robustness against irregular motion and anatomical changes. Significance. This study demonstrates, that real-time adaptive beam delivery strategies can deliver conformal doses within single fractions, thereby enabling hypofractionated treatment schemes that are not feasible with conventional strategies.

Abbreviations

The following abbreviations are used in this manuscript:

Gross target volume CTV Clinical target volume ITV Internal target volume MP4D Multi-phase 4D delivery MP4DRT MP4D with residual tracking **BSRG** Breath-sampled regating **BSRS** Breath-sampled rescanning **BSRT** Breath-sampled retracking TRvCT Time-resolved virtual CT DIR Deformable image registration DVF Deformable vector field CIRT Carbon ion radiotherapy Coefficient of variation CV

1. Introduction

CIRT enables highly conformal treatments of static tumors, thanks to its high geometrical selectivity with respect to conventional radiotherapy (Durante and Loeffler 2010). However, its application on respiratory moving targets in thorax and abdomen is still very limited, mainly due to the interplay effect, causing inhomogeneous dose distributions (Bert and Durante 2011). Additionally, target volume extension to cover the entire range of motion (RoM) leads to a loss in dose conformity. To exploit the full potential of CIRT for moving tumors, motion mitigation strategies have to be established, addressing respiratory motion throughout the treatment planning and delivery course. This study aims to provide insights into the path to go.

The current clinical implementation for motion mitigation is highly heterogeneous and depends strongly on technical capabilities of both the planning software and the delivery system. It includes multiple fields and a high number of fractions, breath-holds and abdominal compression. Plans include large margins or strongly deviating robustness scenarios, as well as density replacements, rescanning, gating or combinations (Zhang et al 2023). These strategies represent a trade-off between conformity, robustness, and the efficiency of delivery and clinical workflow. There appears to be a gap between capabilities of research tools and clinical implementation, where the limitations of clinically available equipment and the lack of information leads to favoring efficiency and robustness over conformity. Especially irregular motion, as observed in patients (Takao et al 2016, Dhont et al 2018), and its effects are understudied especially intra-fractionally. Adaptive therapy can compensate inter-fractional changes (Meijers et al 2020), but also suffers from the lack of time-resolved (TR) three-dimensional (3D) imaging, such that changes in a repeated four-dimensional (4D) computed tomography (CT) (4DCT) could also represent a transient change in breathing pattern. Various motion mitigation strategies were proposed to increase dose conformity and reduce treatment time, including beam tracking and MP4D (Lis et al 2020). In a recent publication, the authors demonstrated a combination of MP4DRT (Steinsberger et al 2023). Application of MP4DRT on a synthetic lung cancer phantom (Segars et al 2008), demonstrated highly conformal and homogeneous dose distributions within a single fraction, even in the case of large and irregular motion, including drifts, while facing realistic errors in tumor motion detection—in contrast to other mitigation strategies (rescanning, beam tracking and MP4D). However, it is yet unclear if this could also translate to a clinically relevant advantage and whether MP4DRT could also be applied to abdominal tumors.

A realistic comparison of various motion mitigation strategies would require imaging data that reflect realistic, TR, 3D anatomical motion, and are suitable for 4D dose calculations. In clinical settings, 4DCT is the standard imaging modality for treatment planning. Nevertheless, 4DCT provides only an average description of respiratory motion during pre-treatment imaging, which is not representative of the breathing variability and/or digestion-induced anatomical changes that might occur within a fraction or between fractions. Magnetic resonance imaging (MRI) has emerged as a modality capable of overcoming this limitation, offering fast, TR image acquisitions (cine-MRI) to capture cycle-to-cycle variations (Paganelli *et al* 2018a). While cine-MRI images provide only bi-dimensional motion information, several studies have investigated methods to obtain TR 3D information, generally relying on motion modeling techniques. Among these, one can implement a correlation model between the motion derived from a 4D imaging modality and cine-MRI—based surrogates (Harris *et al* 2016, Stemkens *et al* 2016, Garau *et al* 2019). Alternatively, TR 3D anatomical information can be estimated as proposed by (Meschini *et al* 2022a), where the motion from 2D cine-MRI is directly propagated in 3D (Paganelli *et al* 2018b) and a reference planning,

end-exhale CT is deformed on the estimated 3D volumes, obtaining TRvCT data suitable for dose calculations.

The aim of this study is to investigate the performance of multiple motion mitigation strategies for 4D delivery in a realistic scenario. This requires image data for treatment planning as well as a separate set depicting the irregularly moving anatomy during actual treatment. To achieve this, the method by Meschini *et al* (2022a) was adopted on five abdominal patients treated with CIRT and undergoing planning 4DCT and cine-MRI acquisitions, in order to derive TRvCT series. These data were used to test the performance of established and innovative motion mitigation strategies in particle therapy for abdominal tumors in a realistic setting, aiming at providing a hint which strategy to choose for treatment schemes between one and 12 fractions and distinguishes between 4D treatment planning strategies and 4D beam delivery methods.

2. Method

2.1. Image data acquisition

This study used five patients with pancreatic (P1 + P2) and hepatic (P3 - P5) localization of disease, treated with CIRT using respiratory gating, at the National Center of Hadrontherapy (CNAO) in Italy. Patient immobilization strategies during treatment planning and delivery, involved customized pillows (MOLDCARE Cushion, QFix Avondale PA, USA) and non-perforated body thermoplastic masks (Klarity Medical Products, USA), applying moderate abdominal compression and reduced amplitude of diaphragm excursion.

Planning 4DCT data were acquired under free breathing using a Siemens SOMATOM Sensation Open CT (Siemens Healthcare GmbH, Germany) scanner with a resolution of $0.98 \times 0.98 \times 2$ mm, along with simultaneous acquisition of a respiratory surrogate signal (AZ–733V system, Anzai Medical Co. Ltd, Japan). 4DCT was retrospectively sorted into eight respiratory phases, namely the end-exhale (0%EX), peak-inhale (100%IN), 50%EX, 50%IN, 30%EX, 30%IN, 20%EX and 20%IN.

MRI scans were obtained on the same day of the planning 4DCT acquisitions, with a 3T scanner (Magnetom Verio, Siemens Healthcare GmbM, Germany). A T2/T1—weighted balanced steady—state free precession sequence (TrueFISP sequence; spacing: 1.33×1.33 mm; slice thickness: 5 mm; repetition/echo time: 228.07 ms/1.5 ms; accelerating factor: 2; acquisition time: 230 ms) was utilized to provide abdominal T2-weighted (T2-w) multi-slice sagittal images in free breathing. These were retrospectively reconstructed according to Meschini *et al* (2019). The resulting volumes consisted of 25 sagittal slices with a limited field of view (FOV) of 12.5 cm in the right–left direction. Additionally, TR 2D cine-MRI consisting of interleaved, orthogonal sagittal/coronal planes intersecting the tumor, were acquired in free breathing for 1.15 min (300 total frames). The study was approved by the local Ethical Committee in CNAO and informed consent for data acquisition was obtained from all patients according to institutional standards.

2.2. Image data generation

For the generation of the TRvCT the method from Meschini *et al* (2022a) was adopted. Even though planning 4DCT and 4DMRI acquisitions underwent on the same day, patient repositioning could potentially cause rigid and non-rigid anatomical variations. In this regard, the 0%EX phase of the T2-w 4DMRI was first rigidly aligned with the corresponding planning 0%EX CT, using the spinal cord as reference. Subsequently a non-rigid registration was performed using a B-spline algorithm (Plastimatch.org), with the resulting DVF extended to encompass the entire FOV of the patient's anatomy (Meschini *et al* 2022b). This DVF was applied on the planning 0%EX CT, yielding a reference vCT.

A DIR pipeline was used to generate the TRvCT series (figure 1). In more detail, an optical flow algorithm was used to deformably register cine-MRI frames on a reference 0%EX cine-MRI frame, yielding 150 pairs of coronal/sagittal 2D DVFs. A one-dimensional (1D) respiratory surrogate signal was derived, in the inferior—superior direction, from the coronal 2D DVFs by calculating the mean displacement within the CTV. Both the 1D surrogate signal and the 2D coronal/sagittal DVFs were interpolated using Piecewise Cubic Hermite Polynomial interpolation, to obtain motion information along the whole time-frame of the acquired breathing signal. From the interpolated 2D DVFs, the fields corresponding to the eight breathing phases of the planning 4DCT were selected and 3D DVFs were reconstructed as done in Meschini *et al* (2022b). Figure 2 illustrates an interpolated surrogate signal derived from an example patient (P1) with the corresponding labels of the reconstructed TRvCT phases, (in appendix the surrogate signals of the rest patients P2–P5 are depicted). Finally, the reference vCT was deformed on the reconstructed 3D DVFs, generating a TRvCT dataset. Negligible spinal cord and rib motion was assumed, because of the abdominal compression exerted during the gating technique, with the propagation applied only to soft tissue organs, as done in Meschini *et al* (2022a).

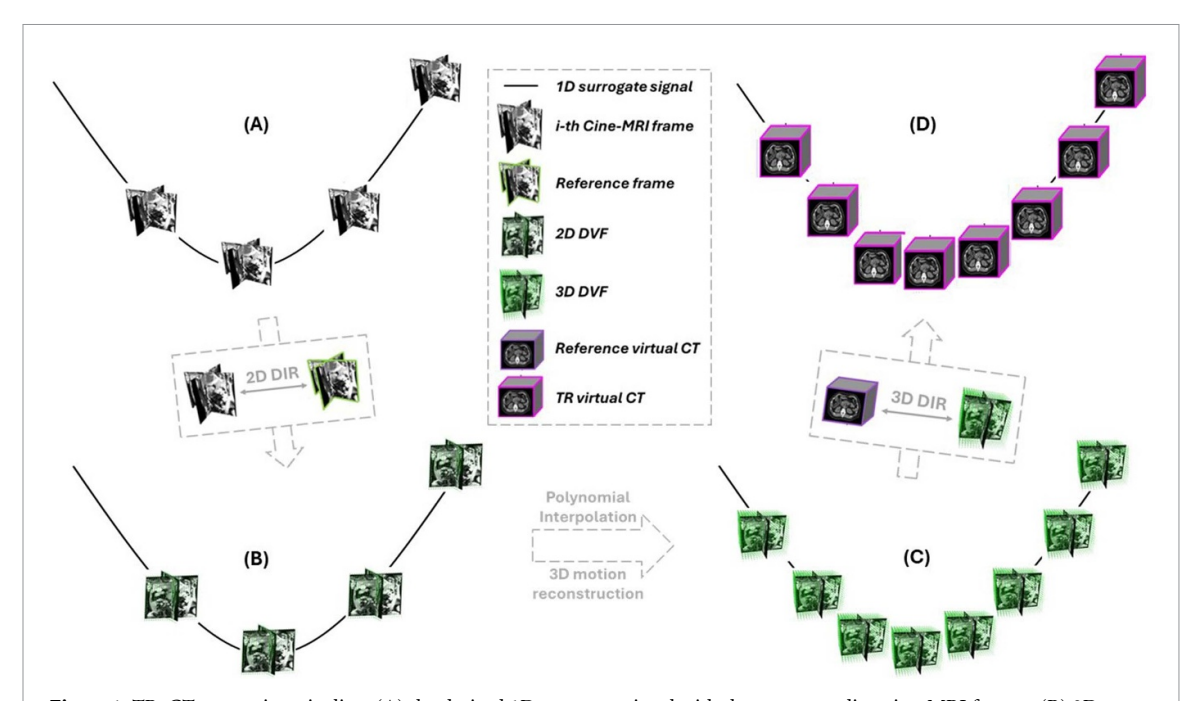


Figure 1. TRvCT generation pipeline: (A) the derived 1D surrogate signal with the corresponding cine-MRI frames; (B) 2D motion information extracted by deforming each cine-MRI frame on a reference frame; (C) interpolation along the whole time-frame and 3D motion reconstruction; (D) warping the reference virtual CT to derive the TRvCT series; for visualization purposes, the pipeline is illustrated for a single breathing cycle.

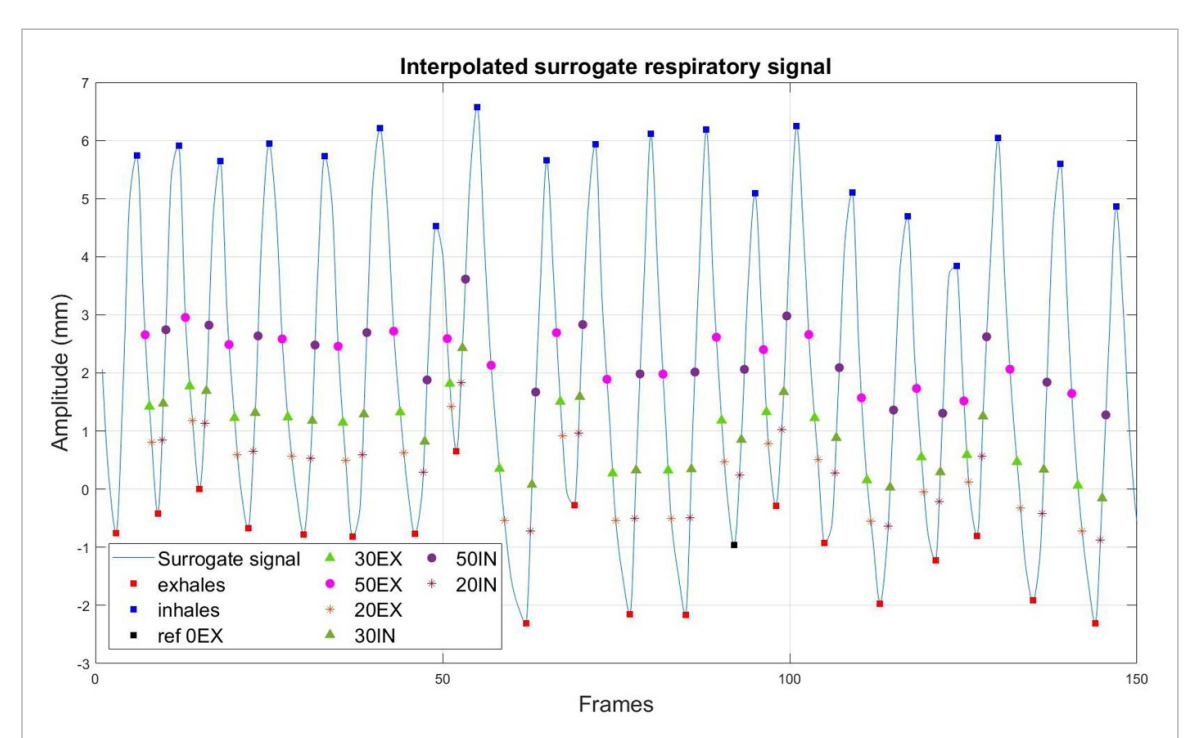


Figure 2. A 1D surrogate respiratory signal extracted from the cine-MRI frames of patient P1, by deformably registering cine-MRI frames on a reference 0%EX frame (ref 0EX). An interpolation step was introduced to obtain motion information along the whole time-frame of the acquired breathing signal.

The cine-MRI data were additionally used to quantify the target's RoM (table 1). For this task, the GTV as defined on the planning 0%EX CT, was propagated on all cine-MRI frames to derive an ITV describing the full motion on cine-MRI, in the inferior–superior direction (Kalantzopoulos *et al* 2020). To quantify the target's motion, the Hausdorff distance was calculated between the generated ITV and the GTV, as the 95th percentile distance over all distances from points in the GTV to their nearest point in the ITV. Table 1 summarizes relevant patient features, including the target's RoM.

Table 1. Patient characteristics and coefficient of variation (CV) in phase and amplitude in the inferior-superior direction.

Patient	Target	Organ at risk	Target volume (cm3)	RoM ^a (mm)	CV-phase (%)	CV-amplitude (%)
P1	Pancreas	Duodenum, stomach	13.83	12.04	15	84
P2	Pancreas	Duodenum, stomach	22.95	4.7	32	73
P3	Liver	Liver, lung	13.14	5.84	38	70
P4	Liver	Liver, lung	8.63	10.94	12	69
P5	Liver	Liver, lung	1.64	8.92	10	74

^a Target Range of motion in the inferior-superior direction.

Furthermore, the percentage of variation in amplitude and phase was derived for all patients, using the CV (table 1). In more detail, differences in amplitude and phase were calculated between consecutive peaks throughout the whole cine-MRI-derived 1D breathing surrogate signal. Then CV was calculated according to the formula:

$$CV [\%] = 100 \times \frac{\text{Standard Deviation (Amplitude or Phase differences)}}{\text{Mean (Amplitude or Phase differences)}}. \tag{1}$$

2.3. Treatment planning

As CTVs had not been delineated for all patients in the study, they were constructed by adding an isotropic 5 mm margin to the contoured GTV and subtracting overlapping OARs as done elsewhere (Zhou *et al* 2023). The contours were propagated to all 4DCT states by DIR using Plastimatch. Treatment plans with two fields were simultaneously optimized on the 4DCT for each patient, using intensity modulated particle therapy. For plan optimization, the GSI in-house software TRiP98 was used (Wolf *et al* 2020, Steinsberger *et al* 2021). Setup errors of up to 3 mm in all three spatial directions and range uncertainties of 3.5% were accounted for by robust optimization (Wolf *et al* 2020) which was also used to avoid steep gradients between the fields. Four optimization strategies were used:

1. **4DITV:** To obtain a plan valid for the entire motion depicted in the 4DCT, also including range changes, the spot weights \overrightarrow{N} are optimized on all M phases of the 4D CT simultaneously (Graeff 2014, Kanai *et al* 2020, Wolf *et al* 2020) by minimizing the cost function

$$F_{\text{Robust 4D}}\left(\vec{N}\right) = \sum_{m \in M} \left[\sum_{i \in \text{CTV}} w_T \times \left(D_{\text{presc.}} - \min_{s \in S} \left(D_{\text{act.}}^{i,m} \left(\vec{N}, s \right) \right) \right)^2 + \sum_{i \in \text{CTV}} w_T^{\text{max}} \times \left(D_{\text{presc.}} - \max_{s \in S} \left(D_{\text{act.}}^{i,m} \left(\vec{N}, s \right) \right) \right)^2 + \sum_{j \in \text{OAR}} w_{\text{OAR}}^{\text{max}} \times \left(D_{\text{limit}}^{\text{OAR}} - \max_{s \in S} \left(D_{\text{act.}}^{i,m} \left(\vec{N}, s \right) \right) \right)^2 \\ \times H\left(\max_{s \in S} \left(D_{\text{act.}}^{i,m} \left(\vec{N}, s \right) \right) - D_{\text{limit}}^{\text{OAR}} \right) \right]$$
(2)

Here $D_{\rm presc}$ and $D_{\rm act}$ are the prescribed and actual dose, and w_T and $w_T^{\rm max}$ are positive weighting factors scaling the penalty of the robustness scenario s with the minimal and maximal dose. The Heaviside step function H is used to score only dose to the organs at risk exceeding the threshold $D_{\rm limit}^{\rm OAR}$ with the corresponding weight $w_{\rm OAR}^{\rm max}$. This strategy was used with all eight 4DCT phases with a minimal spot weight of 25 000 ions for an ITV interplay plan. A four times higher minimum particle limit was used to enable eight times rescanning with half the beam intensity.

- 2. **Gating ITV:** For gated deliveries, plans were optimized using the 4DITV strategy within a gating window, namely on the end-exhale phase and the adjacent 20% inhale and 20% exhale phases, only with a minimum spot weight of 25 000 particles. To combine gating with three times layered rescanning, in the following called regating, plans with at least 75 000 particles per spot were optimized.
- 3. **4D Tracking ITV:** To optimize treatment plans for lateral beam tracking of the tumor center-of-mass (COM), the concept of the 4DITV optimization was extended in this study to optimize plans for lateral beam tracking. This is illustrated in figure 3. Again, each beam spot has the same probability to be delivered in each motion phase. Therefore, the total cost function is the sum of single cost functions in all phases. The same cost function as in equation (2) was used. However, when calculating the matrix relating the spot weights \vec{N} with the dose in relevant voxels, the shift of the lateral spot position expected

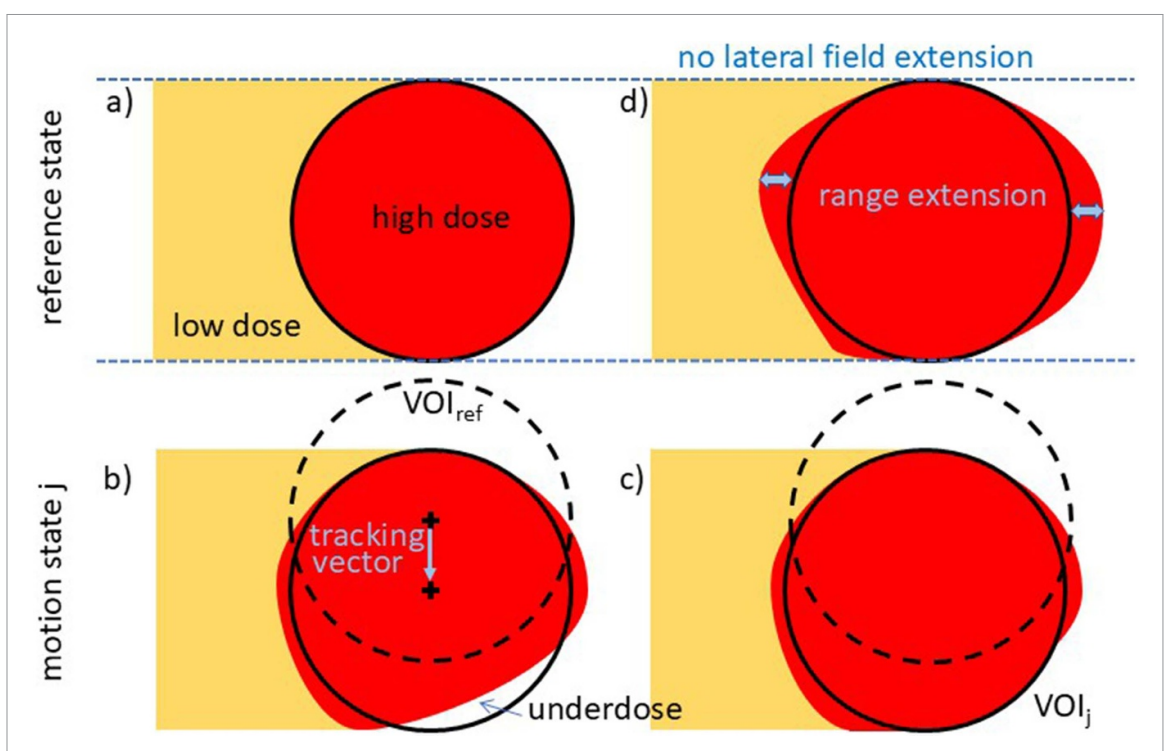


Figure 3. Schematic explanation of the tracking ITV. A plan optimized on the reference phase alone (a) will lead to underdoses due to different beam range if applied to motion phase *j*, even considering a lateral tracking vector (b). Additional optimization of the tracked field in each phase *j* restores target coverage (c), such that the 4D-dose of the full field in the reference phase is conformal in the lateral extension, but adds motion state specific range margins to ensure target coverage in each motion state (d), compare to Kanai *et al* (2020) for a similar explanation of the 4DITV strategy.

to be applied by the dose delivery system (DDS) compensating the tumor motion was taken into consideration. To do so, raster spots were shifted relative to the reference phase by the projection of the tumor COM motion in the plane perpendicular to the beam before calculating the matrix element in the given phase. The rationale behind this approach is that motion induces both a shift of the target relative to the beam and a range change due to traversing different tissue. Lateral tracking can compensate for the first effect, but not the second. The described cost function incorporates range changes similarly to an ITV, but collapses the lateral target size increase by anticipating the tracking vectors. Plans were optimized for a single scan using the same minimum spot weights of 25 000 ions/spot. For a combination with eight times rescanning, denoted as retracking, the spot weight was reduced to 12 500 ions/spot as for the 4DITV. 4D Tracking ITV optimization was implemented into TRiP98 for the purpose of this study.

4. **Single phase uniform dose (SPUD)**: For each of the eight 4DCT phases, a separate treatment plan is 3D optimized to the full prescribed dose with the constraint to use the same set of energies for all phase plans. Finally, the particles numbers in each plan are scaled down by the total number of phases. Therefore, the initial minimum spot weight was increased by a factor of eight to 200 000 ions/spot. All 8 phase plans together form one library.

For all plans, the aim of the optimization was to achieve a target coverage of $D_{95} > 95\%$ with an RBE weighted target dose of 4.8 Gy, mimicking a clinical protocol with 12 fractions. For the pancreatic cancers, the duodenum and stomach were restricted to $V_{75} < 1\%$. For the liver cases, the right lung and liver constraint was $V_{20~\rm Gy} < 20\%$ and $V_{30~\rm Gy} < 33\%$, respectively. The conformity of the dose distributions was assessed by the conformity number

$$CN[\%] = 100 \times \frac{V95_{\text{target}}}{V_{\text{target}}} \times \frac{V95_{\text{target}}}{V95}.$$
(3)

The two fractions describe which fraction of the target is covered by 95% of the target dose and which fraction of the 95% isodose volume is inside the target. Dose inhomogeneity was measured by the difference $D_5 - D_{95}$.

2.4. Beam delivery methods

The following beam delivery techniques were considered.

Table 2. Treatment delivery modalities.

Modality	Optimization	Minimum spot weight/# phases or rescans	Delivery
Gating Regating	Gating ITV	25 000/1 75 000/3	Gating
BSRG			MP4D
Interplay	4DITV	25 000/1	3D
Rescanning		100 000/8	
BSRS			MP4D
Tracking	4D tracking ITV	25 000/1	Tracking
Retracking		100 000/8	
BSRT			MP4DRT
MP4D	SPUD	200 000/8	MP4D
MP4DRT			MP4DRT

- 1. **3D:** The beam is always on when provided by the accelerator.
- 2. **Gating:** The beam is gated when the motion is outside the phase-based gating window defined by the union of the end-exhale phase and the neighboring 20% inhale and 20% exhale phases.
- 3. **Tracking:** The beam is always on when provided by the accelerator. The spot positions are modified laterally to follow the tumor COM.
- 4. **MP4D:** The current motion phase in the breathing cycle is detected. Within the delivery of one iso-energy slice, the DDS switches between phase-specific plans in a library until all phases are entirely delivered. MP4D was first published in combination with SPUD optimization (Lis *et al* 2020). The synchronization can be used to spread rescans evenly over selected fractions or the entire respiratory cycle. This is denoted as breath-sampling (Poulsen *et al* 2018).
- 5. **MP4DRT:** In addition to MP4D, the displacement of the tumor relative to the corresponding motion phase in the 4DCT is tracked laterally.

The treatment planning strategies were combined with these beam delivery methods to form 11 treatment modalities, which are summarized in table 2. 3D delivery, gating and beam tracking were combined with rescanning to obtain native rescanning, regating and retracking. In addition to the native combinations of treatment plan and delivery method (4DITV + 3D, Gating ITV + Gating, 4D Tracking ITV + Tracking, SPUD + MP4D(RT)), the delivery of the rescanning plan using MP4D and the retracking plan using MP4DRT was simulated as well. To do so, the plan libraries were filled with identical plans, each representing one rescan of the optimized plan. The so formed BSRS and BSRT enforce the synchronization of the delivery with the motion. Similarly, MP4D with identical gating ITV plans for all phases inside the gating window and empty plans outside was used to form BSRG. Those three combinations are expected to efficiently mitigate the interplay effect, but increase the treatment time compared to their native delivery mode.

2.5. Dose accumulation

For each patient and delivery mode, 12 fractions were simulated. A periodic repetition of the recorded TR MRI sequence was assumed. The isocenter of the beam was set to the average tumor COM in the 0%EX state in the cycles of the TRvCT. For each fraction, a random setup error \vec{e} was sampled from a 3D Gaussian distribution with a confidence level of 90% for $|\vec{e}|$ and added to the target point. For each field and fraction, a random start phase of the delivery was sampled with setup error and start phase being identical over all simulated treatment modalities. The RBE-weighted dose was accumulated on a reference virtual CT using an algorithm capable to handle arbitrarily long imaging series (Steinsberger *et al* 2021). Based on the time, the current image of the TRvCT series and corresponding motion phase was determined. The beam delivery sequence was simulated dependent on the beam delivery method. As accelerator time structure, a maximum extraction time of 3 s, a spill pause of 2.3 s and an energy-dependent, but constant particle rate of $(2.8-6.5)\times 10^7$ ions \cdot s⁻¹ were used, as measured at CNAO. In order to map the dose contributions calculated on single virtual CTs to the reference virtual CT, the 3D DVF described in section 2.2 were inverted using Plastimatch. For the purpose of dosimetric evaluation, a non-rigid registration (through Plastimatch) was also performed to map the contours from the planning CT to this reference virtual CT. The

quality of single fractions was evaluated considering target coverage (D_{95}) and homogeneity $(D_5 - D_{95})$ in CTV and GTV and the dose to the organs at risk.

In order to investigate how suitable a motion mitigation strategy is for a hypofractionated treatment, not only the dose in a single fraction is of interest, but the sum accumulated over several fractions. Random interplay patterns are expected to be averaged when accumulating several fractions while systematic target miss is expected to remain. For each patient, convergence was estimated by calculating the DVH after k = 2, 3, 4, 6, 8, 12 fractions. For k = 2, 3, 4 fractions, all distinct combinations to pick k fractions out of the 12 simulated dose distributions including repetitions were simulated by adding up the corresponding dose distributions and calculating the DVH metrics using an adapted RBE-weighted target dose of $k \times 4.8$ Gy. The results were weighted by the number of permutations of selected fractions as done by Poulsen *et al* (2018). In order to save computation time, the accumulated dose at later time-points was calculated for 100 random sequences of random integers between 1 and 12 with the length being the number of fractions. The same set of 100 sequences of single fraction doses was used for all motion mitigation strategies.

2.6. Experimental validation

To verify the results, the treatment plans for patient P4 were delivered to a moving phantom with the experimental 4D DDS CNAO described in our previous publications (Lis *et al* 2020, Steinsberger 2022, Steinsberger *et al* 2023). The horizontal beamline of the experimental room was used for this. The phantom consisted of an ionization chamber array detector (Octavius 1500XDR, PTW, Freiburg, Germany) on a moving stage (M-414.2PD, Physik Instrumente, Karlsruhe, Germany). The stage performed cyclic repetitions of the tumor COM trajectory recorded in the TRvCT series for the patient. The corresponding motion state was recorded. The 4D dose distributions were reconstructed by extracting the time structure, beam current, measured beam position and TRvCT state from the log-files of the DDS and accumulating the 4D delivered dose on the reference virtual CT as it was done in the simulations. The accuracy of the method was already demonstrated in previous publications (Steinsberger *et al* 2021, 2023).

3. Results

In the following, the results for liver patient P4 are presented for illustration. This patient was also selected for the experimental validation because its relatively large tumor motion and as the more loose dose constraints compared to the pancreatic cases facilitates the focus on interplay effects. The results include planned dose distributions on the 4DCT, simulated single fractions calculated on the TRvCT and dose reconstructions calculated on the TRvCT using timings and spot positions as logged during the experiments. Then, simulation results for fractionated treatment courses are presented for all patients. Notably, the analysis of motion variation highlighted distinct differences in both phase and amplitude, among and within individual patients (table 1), underscoring that each patient exhibits unique characteristics. This diversity enhances the robustness and relevance of the analysis, allowing for a more meaningful understanding of patient-specific differences in treatment response.

3.1. Experimentally evaluated case P4

The log-file-based 4D dose reconstructions of the experimental deliveries for patient P4 are illustrated in figure 4. In figures 5 and 6, the target coverage and dose homogeneity for P4 is depicted. The planned 4D dose distributions (dotted lines) all fulfilled the acceptance criterion of $D_{95} > 95\%$. Simulated single fraction doses (markers and boxes) deviate strongly for the planning because of interplay and anatomical changes between planning 4DCT and TRvCT images. For beam gating, 4DITV and beam tracking plans, rescanning led to a clear improvement of both target coverage and homogeneity, which is further enhanced by breath-sampling through the use of the MP4D and MP4DRT delivery technique. Reconstructed CTV coverage and dose homogeneity deviated from the range of simulated values by a few percent, but are sufficiently close to lead to the same conclusions when comparing between modalities. The averaging effect of the accumulation of 12 fraction doses lead to an increase in target coverage and a reduction of dose inhomogeneity. This gain was higher for single scan deliveries and still substantial for combinations with rescans. For the breath sampling, the summed dose was only slightly better than single fractions with the exception of BSRG. Here, the target coverage of the summed dose was even inferior to the median of single fractions, but well within their range. D_{95} and $D_5 - D_{95}$ calculated based on the machine log-files of the experimental deliveries (dashed lines) are compared to the pure simulations in figures 5 and 6. Most values are within the range of the simulated fractions and all of them confirm the trade-offs made between deliveries with same optimization, but different optimization strategy.

The experimentally measured delivery times are displayed in figure 7. As the gating window was open for three out of eight motion phases and the maximum extraction time was in the order of the breathing period,

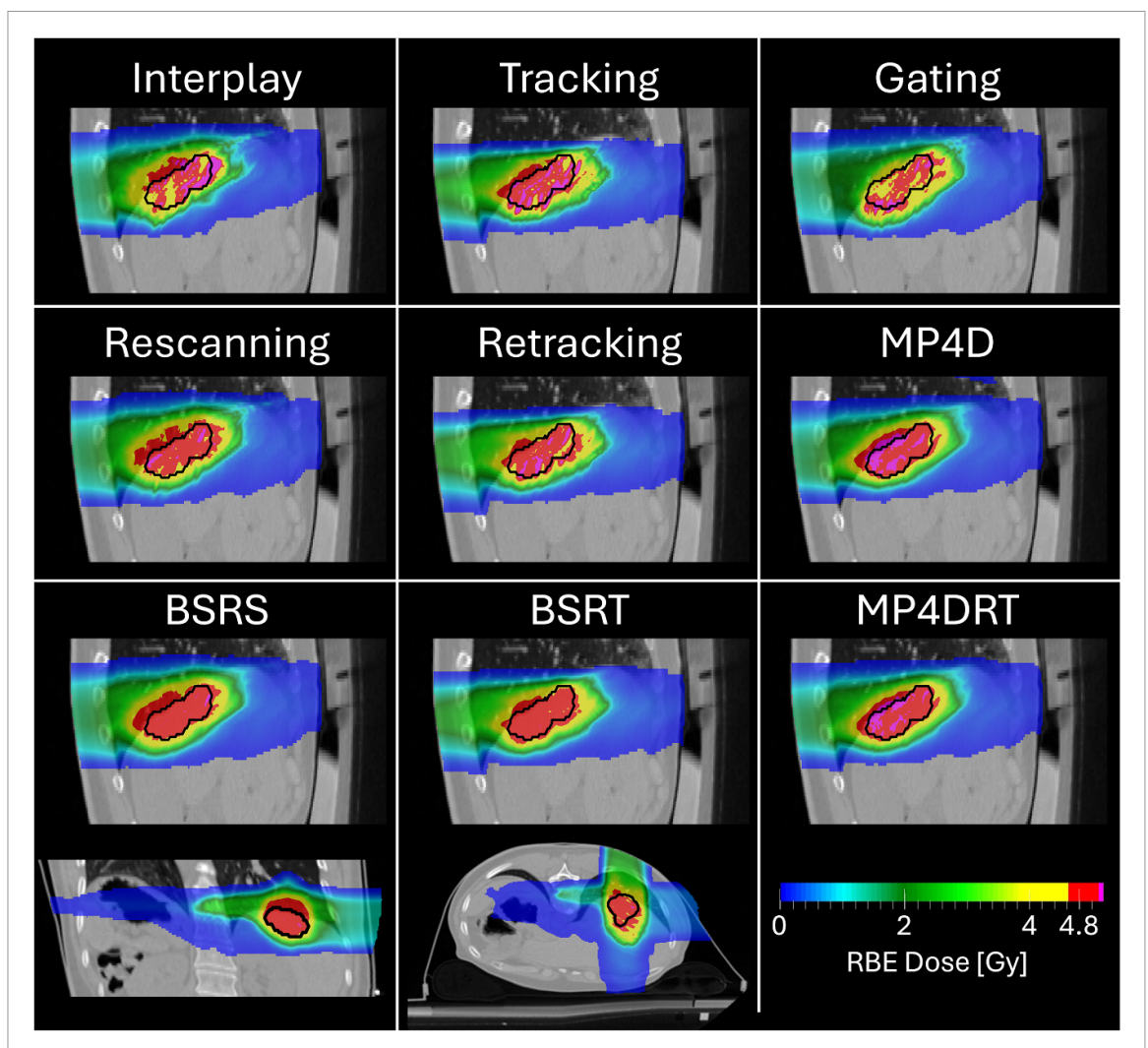


Figure 4. Sagittal slices of the dose reconstructions of the experimental deliveries for P4. For BSRS and BSRT, an axial and a coronal slice where added to illustrate the geometry. The black contour labels the CTV. In the background, the reference phase of the TRvCT is shown.

there was sufficient overlap between extraction from the synchrotron and the time in the gating window to deliver all points of most iso-energetic slices within one synchrotron cycle. Consequently treatment time was dominated by energy switching times of the synchrotron and gating was only slightly slower then interplay and beam tracking. While the reduced beam intensity leads only to a minor increase in treatment time of retracking compared to beam tracking, rescanning takes much longer than interplay. This can be understood by the fact that the larger treatment volume of the 4DITV yields a larger particle number per slice and broke often the threshold which could be delivered during one 3 s long spill. Breath-sampling led to an increase in treatment time by approximately a factor of two compared to normal rescanning. Among the breath-sampled techniques, the SPUD plans (MP4D and MP4DRT) had the smallest total number of particles and the shortest delivery times.

3.2. Treatment planning

The considered DVH metrics of the planned 4D dose distributions are illustrated for all patients in figure 8. The aimed CTV coverage of $D_{95} > 95\%$ was achieved in all cases, except for the pancreatic cancer case P2 in which the tumor was too close to the duodenum. The OAR doses (figure 11) were critical only for the pancreatic case P1, where it was highest for the 4DITV plans. In this case, the requirement $V_{75} < 1\%$ could not be fulfilled for the gating ITV and 4DITV plans, but for 4D tracking ITV and more clearly by the SPUD optimization strategy. The conformity number was highest using the 4D tracking ITV for patients P2, P3 and P4. For P5, the highest CN was achieved for the gating ITV with a small advantage compared to the SPUD optimization, which was the most conformal one for P1.

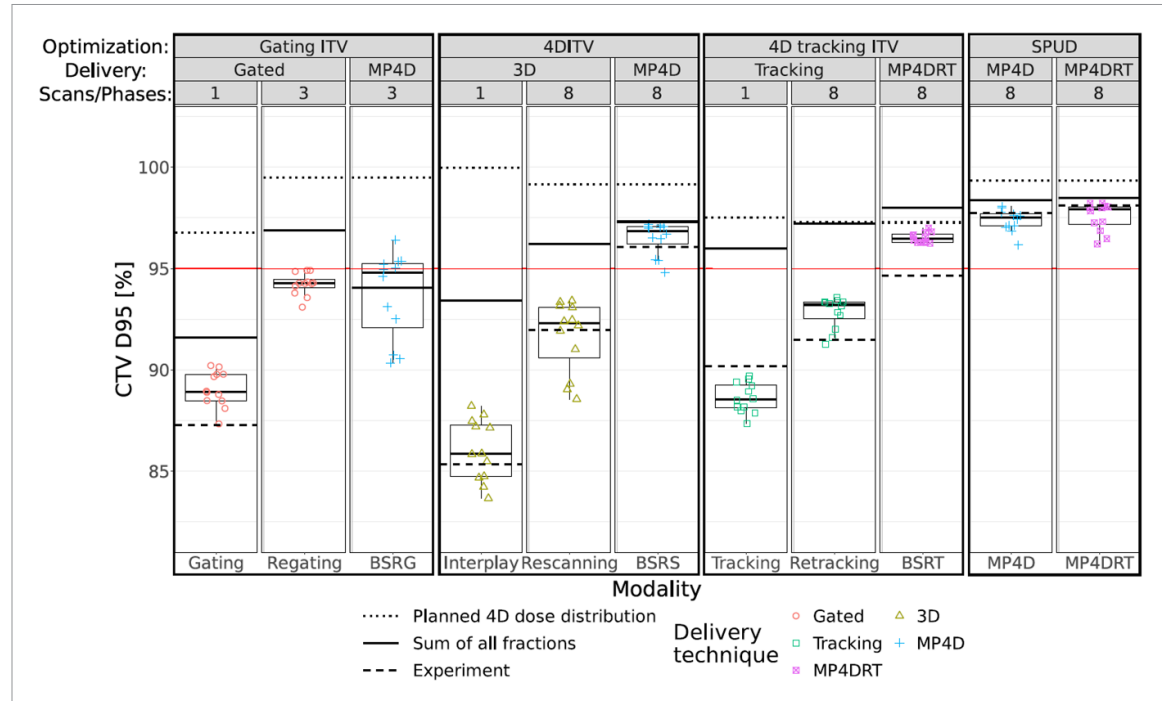
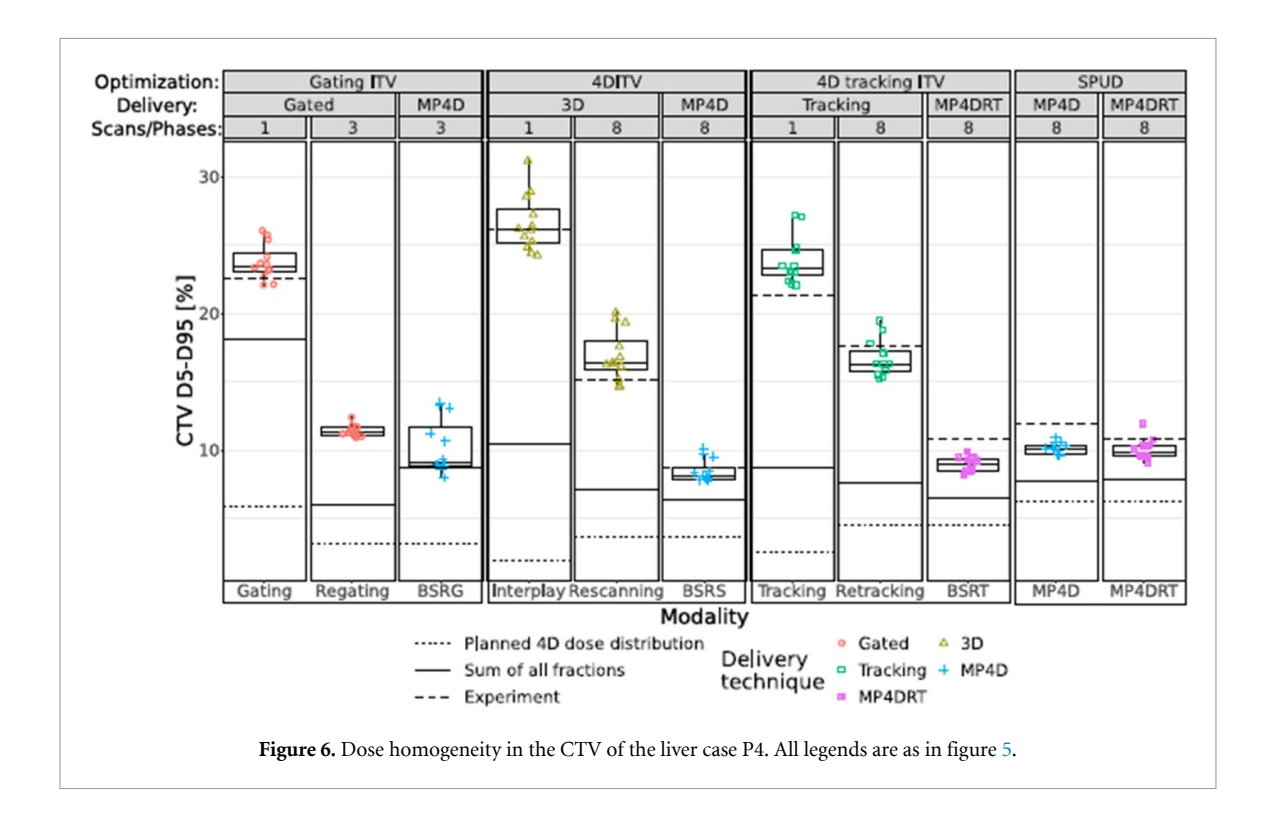


Figure 5. Target coverage of the CTV for the liver case P4. Markers and boxes denote simulated treatment fractions. Marker shape and color correspond to the delivery technique. The black horizontal lines correspond to the value of the planned dose distribution (dotted), the sum of all 12 simulated fractions (solid) and the value obtained from the log-file based dose reconstruction of the experiment (dashed, not regating and BSRG). The red horizontal line represents the acceptance criterion of $D_{95} > 95\%$. Treatment modalities with the same optimization strategy and the same number of scans or phases have identical planned 4D dose distributions.



3.3. Simulated deliveries on TRvCT

Figure 9 displays the evolution of the considered dose metrics for the CTV over the course of a fractionated treatment. Bands illustrate the 90% interquartile range. For all metrics and motion mitigation strategies, a convergence of the metrics with increasing number of fractions is observed. Because of the anatomical changes, the difference in motion pattern between planning 4DCT and MRI sequence, and the interplay effect, the delivered dose distributions differ strongly from the planning. As the anatomical changes affect all dose calculations for a patient systematically, but are different for each patient, the obtained curves converge

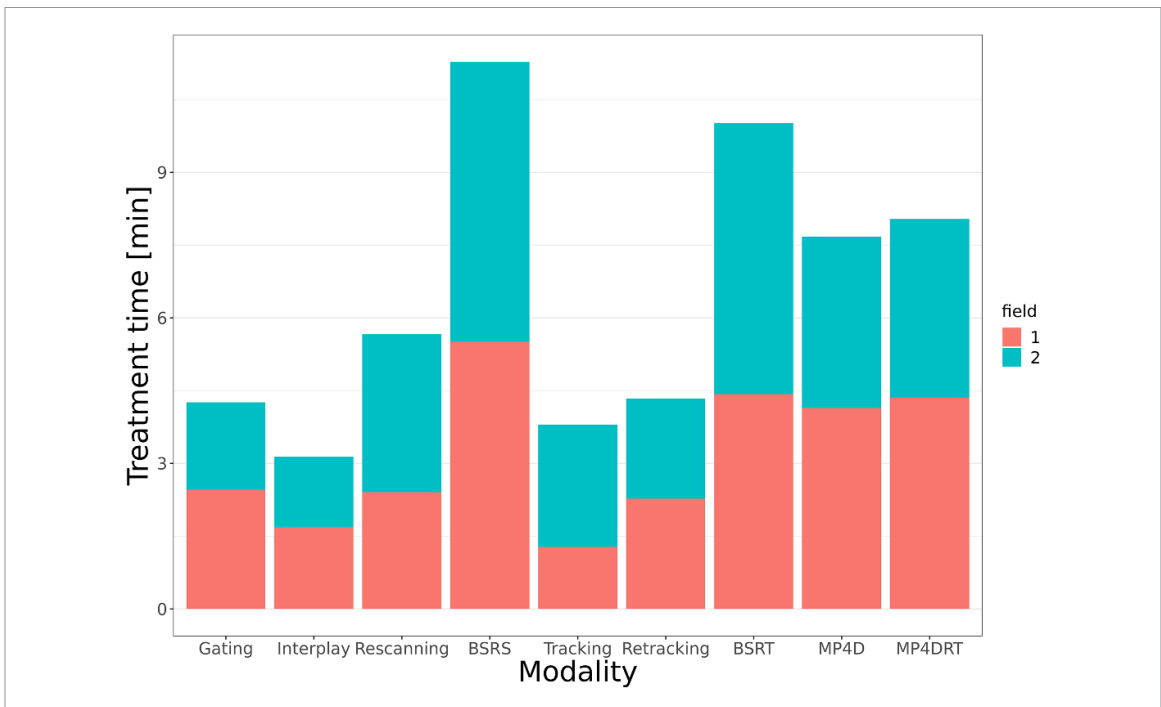
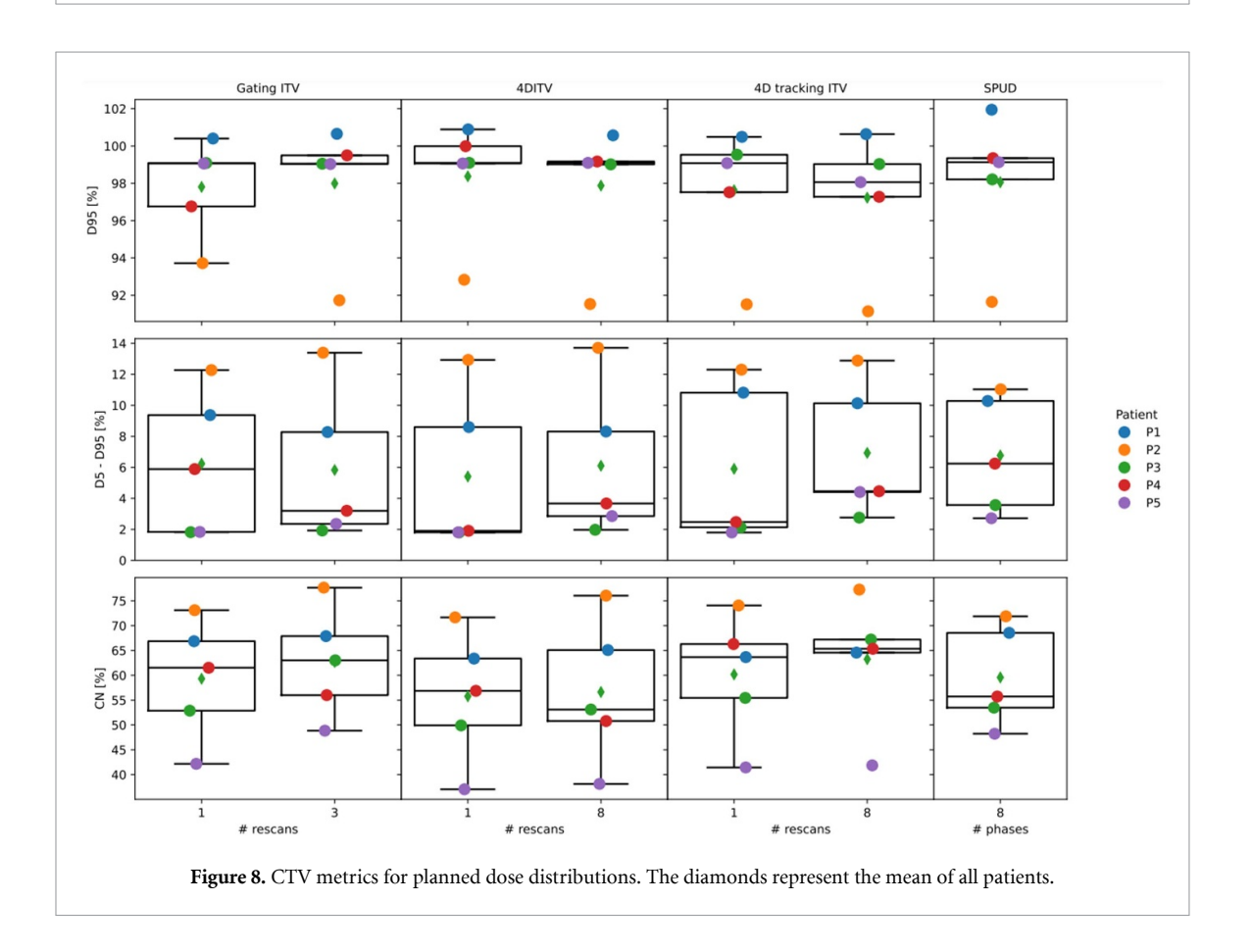


Figure 7. Treatment times during the experiment defined as time from the DDS entering the treatment state until the completion of the last spot of the field.



against different final values. Apart from this offset, the shapes of those curves are similar across patients. It can be observed, that the 90% bands are systematically thinner for breath-sampled techniques compared to the other techniques. This indicates a higher reliability of those methods. An exception is P2, for which a range shift in one of the fields caused a strong loss of CTV coverage for all treatment modalities. Thus, this patient is considered as requiring replanning and is therefore excluded from the further analysis. For each patient and treatment modality, the average dose metric converges towards better values with an increasing

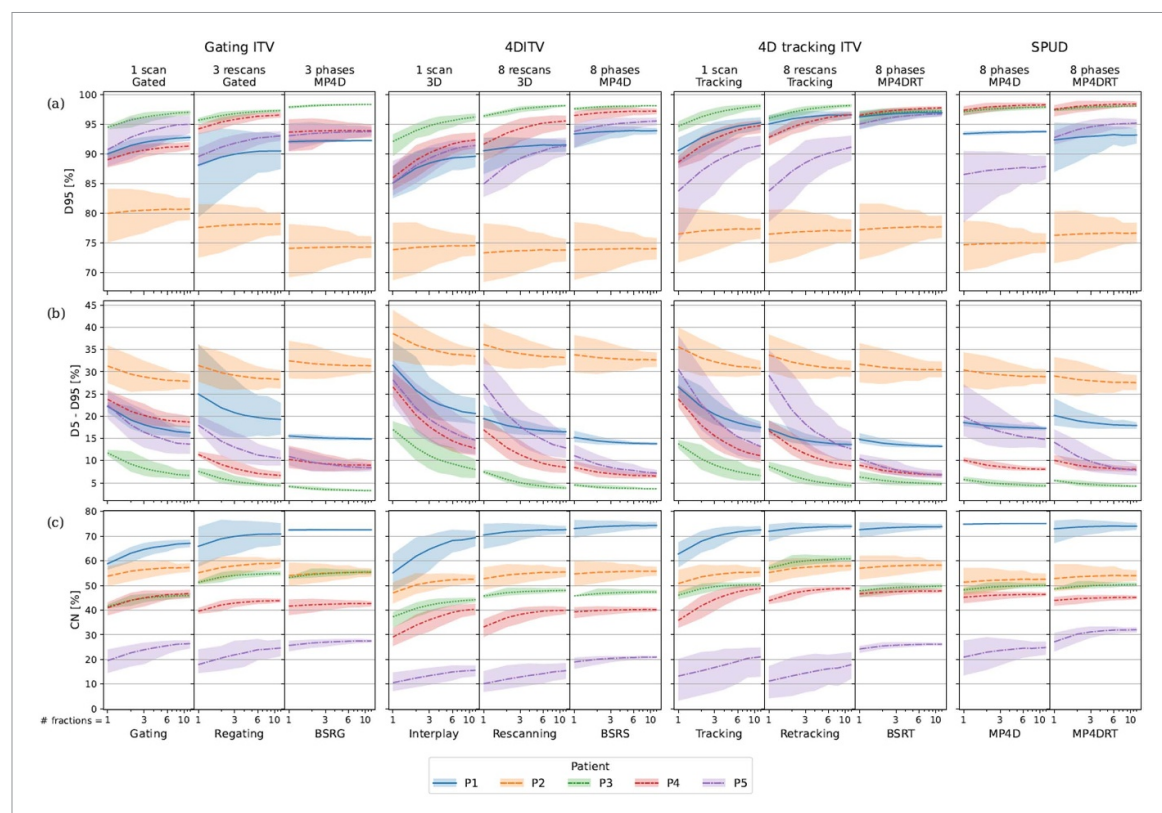


Figure 9. Course of target metrics over the course of a fractionated treatment. Lines illustrate the mean values. Bands represent the 90% band (quartiles 5%–95%). (a) D_{95} target coverage, (b) dose homogeneity ($D_5 - D_{95}$), and (c) conformity number (CN).

amount of fractions. At the same time, the interquartile range decreases. Compared to the other modalities, the phase-based treatment modalities consistently show high dose coverage and low $D_5 - D_{95}$ already starting from the first fraction. An exception is MP4D for patient P5, for which the motion irregularity caused a clear loss of CTV D_{95} . Most striking is the high consistency of D_{95} for BSRT compared to the other modalities.

Figure 10 depicts the evolution of the target metrics averaged over all patients except P2 to clarify the general trend: For all three metrics, the phase-based treatment modalities (green) dominate over rescanned (orange) treatments and deliveries with only a single scan per fraction (blue).

Figure 11 illustrate the OAR metrices on a per patient base. For the three liver cancer cases, the mean dose the healthy liver was clearly below the constraints and therefore plays a minor role. For the pancreatic cases, however, it was challenging to fulfill the constraint of duodenum $V_{75} < 1\%$. For P2, it could be achieved during optimization while sacrificing target coverage (see appendix), but the anatomical change between planning 4DCT and TR MRI reduced the dose in the duodenum for all treatment deliveries far below this threshold. For P1, in contrast, the constraint could be fulfilled only with the 4D tracking ITV and SPUD optimization strategies. During treatment, only the SPUD modalities MP4D and MP4DRT could fulfill the constraint. The constraint was violated most severely by the 4DITV deliveries and regating. For all patients and modalities, the interquartile ranges decreased with increasing number of fractions, but except for P2, there was only little improvement of the average.

4. Discussion

In this study, the efficacy of 11 different motion mitigation strategies in scanned CIRT was assessed in a realistic scenario, using imaging data capturing irregular motion patterns. A dedicated pipeline was applied on five abdominal patients, in order to generate TRvCT series, animated with motion information derived from 2D cine-MRI. This dataset presented variability both in terms of amplitude and phase, up to 84(%) and 38(%), respectively. Although dose calculation on TRvCT generated from TR MRI sequences is similar to other recent publications in the field (Duetschler *et al* 2022, Meschini *et al* 2022a, Hamaide *et al* 2023), the presented study is, to the best of our knowledge, the first analysis comparing the efficacy of such a variety of different motion mitigation strategies for scanned ion beam therapy. The different amount of fractions also enables a perspective on the usability of the investigated motion mitigation strategies for hypofractionated treatment schemes.

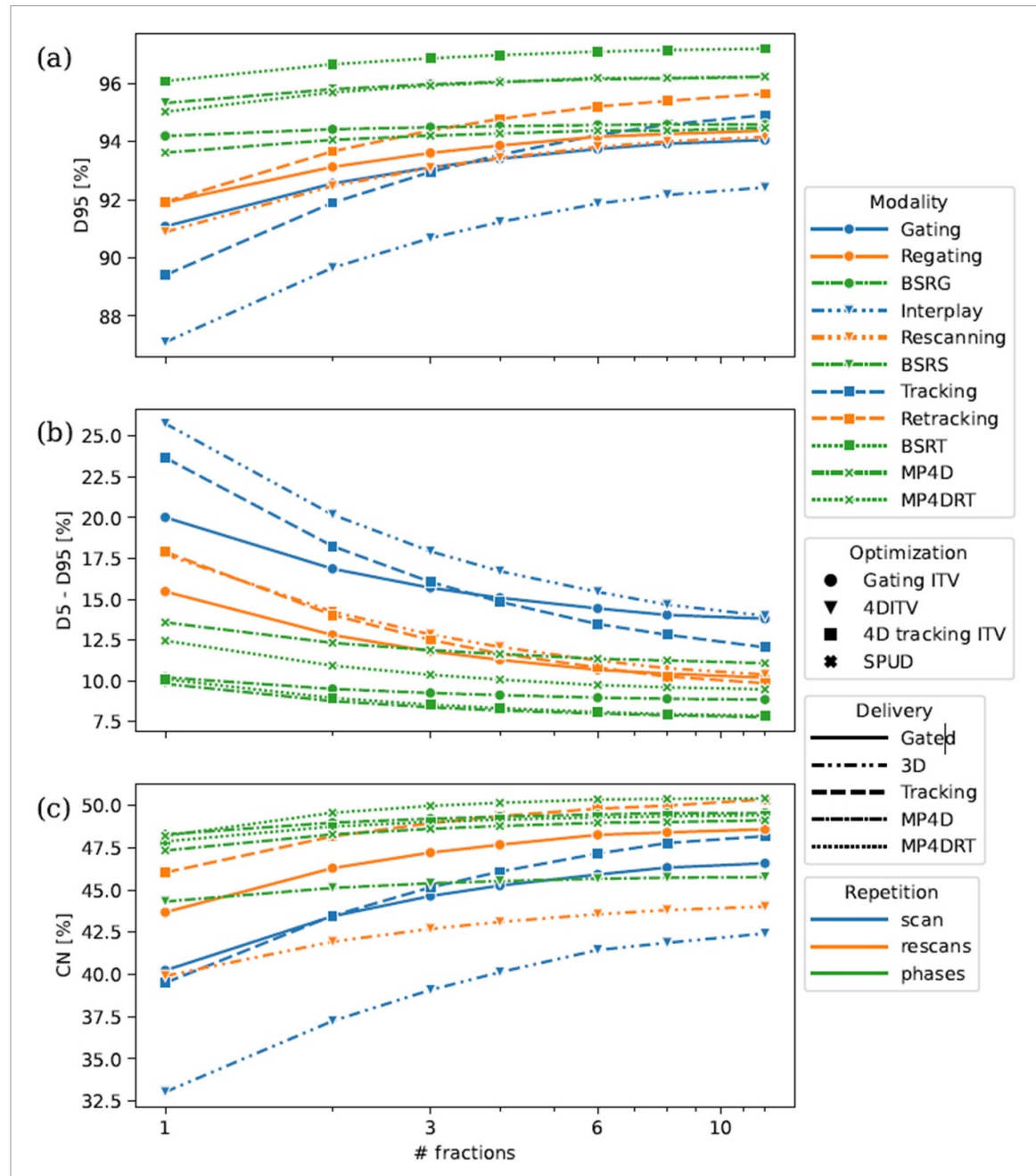


Figure 10. Average course of CTV metrics of all patients except P2. Markers code the optimization strategies, line styles represents the delivery technique. Color represents if a single scan was used (blue), rescanning was applied (orange) or if one of the phase-based delivery methods was used. (a) D_{95} target coverage, (b) dose homogeneity ($D_5 - D_{95}$), and (c) conformity number (CN).

Of course, even more combinations are thinkable. For example, it would be possible to restrict the active phases of all motion mitigation strategies using MP4D and MP4DRT delivery to a gating window as it was done for BSRG in this work. As proposed by the author (Steinsberger 2022), the MP4DRT delivery technique might enable gated deliveries that are robust against baseline drifts or difficult to reproduce tumor positions during breath-hold treatments. However, as neither large drifts nor images of breath-hold were available, this was out of scope for this work.

4.1. Ranking of the treatment modalities

The results were strongly patient-specific, making it challenging to draw clear recommendations from the sample size studied. Still, under this proviso, the authors argue for the following preliminary ranking:

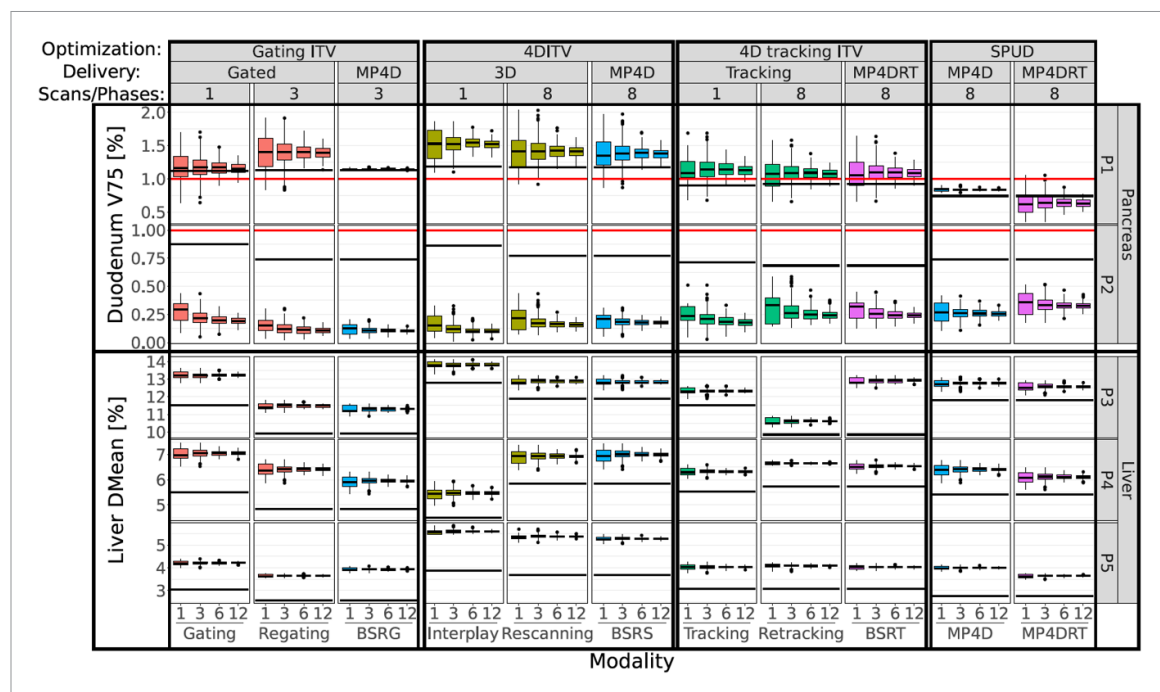


Figure 11. V_{75} in the duodenum for the pancreatic cancer patients and Dmean for the liver cancer patients depending on the treatment modality and the number of fractions calculated on the TRvCT. The horizontal line represents the planned 4D dose distribution.

1. Rank: BSRT:

- BSRT reaches the highest target coverage.
- Target coverage is most consistent among patients
- The performance is high starting from the first fraction with low dependency on the starting phase.
- Together with MP4DRT, the achieved homogeneity in the target is highest. The difference between those two modalities is marginal.
- Considering dose conformality, BSRT is inside a close leading group.

2. Rank: MP4DRT:

- Second in rank, considering target coverage.
- MP4DRT is more conformal than BSRS.
- MP4DRT achieves a higher dose homogeneity than each non-phase based modality.
- For P1, which was the only patient, for which the OAR doses where critical during delivery, MP4DRT achieved the lowest V_{75} for the duodenum.

3-5. Rank: shared by MP4D, BSRS, and BSRG:

- Among those three, BSRS reaches the highest target coverage as it is most robust against irregular motion.
- MP4D has the best conformality. Especially for P1, the advantage in OAR sparing is crucial.
- BSRG lies between the two other techniques for those metrics.

6. Rank: retracking:

- Among the non-phase based modalities, retracking achieves the best conformity and target coverage.
- For more than three fraction, the target coverage with retracking is even higher than for BSRG.

7. Rank: regating:

• For regating, target coverage and conformity is slightly inferior to retracking while dose homogeneity is superior. It does not profit from fractionation the same way as retracking, but converges against inferior values.

• In this study, a phase based gating method was used. More common is amplitude based gating or a treatment with breath-hold. It can be expected that amplitude based gating yields better dosimetric results at the expense of increased treatment times and the risk of required repositioning during treatment in the case of a baseline drift.

8. Rank: tracking:

- After more than eight fractions, tracking achieves a target coverage higher than BSRS with medium homogeneity and conformity.
- Even after 12 fractions, the average curves still have a relatively high slope, suggesting that tracking would benefit from an even higher number of fraction, which is common for most many indications.
- However, it is not suitable for hypofractionated treatments.
- In any case, it is inferior to retracking, which can be achieved with similar requirements on treatment planning and DDSs.

9. Rank: rescanning:

- The target with rescanning coverage is similar to tracking.
- Dose homogeneity is superior to tracking, even comparable to retracking.
- Dose conformity and OAR sparing in the critical case P1 is clearly inferior to tracking.

10. Rank: gating

- The high vulnerability of gating to irregular motion causes problems in all considered metrics.
- Even during planning, gating did not achieve the best OAR sparing. It is not guaranteed that the phase one is gating on is also the best one to protect the OARs.
- As for regating, the results for gating are subject to the proviso, that phase-based gating was used.

11. Rank: interplay:

- In all considered target metrics, a 4DITV delivery without motion mitigation yields the worst results.
- After 12 fractions, the curves still show a convergence towards better values, suggesting an improvement for a larger number of fractions. However, the deficit in target coverage compared to all other techniques is so high, that it is improbable that it will catch up with most treatment schemes.

4.2. Conceptional conclusions

Several conclusions can be drawn regarding the core principles of 4D dose optimization and beam delivery in scanned ion beam therapy:

- 1. Breath-sampled deliveries are recommended, especially for hypofractionated treatment schemes. Irrespective of the treatment planning strategy, the breath-sampled showed clear advantages over single scans for all patients. Compared to layered rescanning, the advantage depends on the patient and in some cases vanished after several fractions. When using three or less fractions, the target coverage of single fractions is crucial considering the uncertainties in biological dose accumulation. In this study, the MP4D and MP4DRT beam delivery method was applied to enforce BSRS. It still has to be investigated if, and how much, the achieved improvement in motion mitigation differs from the phase-controlled rescanning strategy (Furukawa *et al* 2007), which was shown to be efficient even in the case of irregular motion periods (Mori and Furukawa 2016).
- 2. Among the considered optimization strategies, the 4DITV plans were the least conformal ones. As this is already an advanced ITV optimization that also considers the OAR motion in the 4DCT, this is expected to translate also to less sophisticated approaches like the definition of geometric ITVs with density override.
- 3. Gating is more susceptible to anatomical changes than other motion mitigation strategies as it relies on only few phases of the breathing cycle. The residual motion inside the gating window led to non-negligible interplay which could be mitigated by combining it with rescanning. This result is in agreement with other studies (Zhang *et al* 2015).

- 4. Beam tracking alone has low efficacy in mitigating interplay. Compared to the 4DITV, the irradiated volume could be reduced, but the interplay within the target, caused by the range changes and non-translational motion components, is on a similar level as without tracking. Similar to 3D deliveries, in some cases this can be mitigated by layered rescanning. A delivery of 4D tracking ITV plans with the MP4DRT delivery technique, however, solves this problem on the expense of an increased treatment time.
- 5. The 4D tracking ITV optimization strategy was presented for the first time in this work. The dose distributions obtained by using the resulting plans in BSRT or after several fractions demonstrate the potential of this technique to be used for multi-field optimization. The direct comparison between BSRT and native MP4DRT showed that the outcome was quite similar and depends on the patient and considered metric. A potential advantage is that for the 4D tracking ITV plan, the number of rescans for spots with low particle weight can be reduced by removing them from some phases, for example in a manner similar to the one proposed by Poulsen *et al* (2018).

4.3. Strengths and limitations

The limited number of investigated patients limits the statistical power of the given study. Further investigations on a larger patient cohort will therefore be necessary, also including repeated TR MRI acquisitions.

This study uses different image series for treatment planning and 4D dose accumulation. This resembles the real clinical situation where the anatomy may change between planning CT acquisition and delivery. It therefore removes the unrealistic bias towards highly conformal treatment planning strategies present in studies using the same dataset. Instead it challenges the robustness of the treatment plans. At the same time, it might introduce a negative bias. Anatomical variations between planning 4DCT and TR MR sequence and artifacts in the image generation always affect the dose distributions in the same way. For example in patient P2, a range change in the digestive tract caused a systematic and unacceptable loss in dose coverage of the CTV. In a real case, this is expected only in few, but not all fractions, otherwise different sections of the target might be affected. Possibly, an online cone-beam CT would have also triggered a plan adaptation.

As the same image series with a length of 1.15 min was repeated, no major baseline drifts were observed for the investigated patients, but would be expected in a real case (Takao *et al* 2016, Dhont *et al* 2018). This bias favors beam delivery methods without beam tracking as previously shown (Steinsberger *et al* 2023). Therefore, at least for patients prone to baseline drifts, beam tracking is expected to be a reasonable safety feature. In order to simulate the beam delivery using the breath-sampled techniques, TRvCT images were generated for discrete motion phases in a cycle. To include gating into the study without having to use different imaging data, a phase-based gating was used. In clinical practice, however, gating is performed based on an amplitude window. Assuming a good correlation between observed surrogate and internal tumor motion, this reduces the residual motion, but also beam-on time. Consequently, the presented study is expected to overestimate motion artifacts and underestimate treatment times in the gated deliveries.

The selected field angles were limited to horizontal and vertical fields in order to comply with the available fixed beamlines at CNAO. This limitation is not given for other treatment facilities using gantries, 45° fields or were the patient couch can be tilted. Especially for pancreatic cancer, oblique beams were recommended (Batista *et al* 2017, Zhou *et al* 2023) to reduce the impact of range changes.

The study uses carbon ions. Because of their smaller spot size and higher peak-to-plateau ratio, they offer more conformal dose distributions than protons, but are more sensitive to interplay and anatomical changes. From our study, we predict that breath-sampling would improve dose distributions also for protons compared to standard rescanning as also reported by Poulsen *et al* (2018), but the effect will be smaller, especially for normally fractionated treatments.

Plans were only delivered with single fraction doses. Especially the effect on treatment times for hypofractionated treatment schemes remains unclear. However, a change in favor of the MP4D and MP4DRT delivery method can be expected. This can be understood by the fact that the treatment time of MP4D for low doses is dominated by the gating times within phases. An increase in dose does not increase treatment time until the critical point is reached when slices of single phase plans cannot be delivered within one occurrence of the phase. Therefore, up to this point, the efficiency of MP4D during beam-on time increases with dose. The corresponding critical point, when two breathing cycles are needed per slice is at a lower dose for beam gating. In general, the critical points depend on particle rate and breathing period and are therefore patient and facility specific and might even vary in between days (Lebbink *et al* 2022). Further investigation of those parameters is therefore necessary.

In this study, RBE weighted dose distributions from single fractions were added linearly. This discards the biological uncertainties related to tissue response. As these uncertainties are even higher for inhomogeneous

IOP Publishing

dose distributions and point doses varying from fraction to fraction due to interplay, the clinical experience gained from static tumors can most easily be transferred to moving tumors to the breath-sampled motion mitigation techniques providing homogeneous doses in single fractions.

4.4. Clinical applicability

Currently, to the best knowledge of the authors, real-time adaptive beam delivery is not yet available in commercial DDSs for particle therapy. However, lateral beam tracking, MP4D, and MP4DRT will be available in future versions of the clinical DDS at CNAO (Donetti et al 2021). The research prototype used in this study demonstrated the technical feasibility, even facing the uncertainties that can be expected from realistic motion monitoring systems (Steinsberger et al 2023). Phase-controlled rescanning by adapting the dose rate as implemented elsewhere (Furukawa et al 2007) might be a more easily accessible way to achieve breath-sampled deliveries. The missing ability to deliver treatment plans with those techniques prevented the implementation of dedicated treatment planning strategies such as SPUD and tracking ITV in commercial treatment planning systems. But as the concepts are described in literature and their implementation was demonstrated to be feasible within TRiP98, their implementation is considered as the minor challenge compared to the dose delivery. Additionally, the good target coverage achieved by BSRS demonstrates, that MP4D dose delivery can also be used with more conventional treatment strategies, reducing the challenges during clinical implementation.

5. Conclusion

In this study, TR MRI data were exploited to evaluate the performance of 11 different motion mitigation strategies in CIRT of abdominal tumors. TRvCTs were created in order to provide a dataset consisting of non-periodic imaging data, suitable for dose calculations. The studies aimed at providing hints for the right choice of motion mitigation modality for abdominal patients, although analyses strongly depends on patient characteristics and need to be extended on a larger patient cohort. Nevertheless several key observations where made which guide the path for future investigations:

For cases with organs at risk very close to the tumor, real-time adaptive beam delivery strategies using MP4D and MP4DRT or beam tracking can bring the decisive advantage in conformity compared to gating and or ITV deliveries. However, the conformity makes them also more susceptible to anatomical changes. So online imaging to verify the suitability of the treatment is required. The extra effort for this, together with the effect on treatment time, make those highly conformal treatment modalities mainly beneficial for hypo-fractionated treatment schemes. For those cases, also the time efficiency of MP4D and MP4DRT is more affordable. At the same time, highly efficient averaging of breath-sampled techniques yields the highest effect. As beam tracking is a crucial safety measure in case of irregular motion, especially for baseline drifts, the authors recommend the use of the MP4DRT delivery technique. The choice of the optimization strategy is a patient specific trade-off between SPUD and 4D tracking ITV.

For normally fractionated treatment schemes and the motion amplitudes for the patients in this study, 4DITV rescanning or regating appear sufficient. The choice of the technique can be done on the already well established modalities. In cases, when a baseline drift would cause critical dose in an OAR, however, real-time imaging of the tumor position is necessary anyways, such that retracking becomes a valid option. The same holds true for larger motion amplitudes, when gating loses time efficiency and the loss of conformity of ITV treatments becomes unaffordable.

Data availability statement

The data cannot be made publicly available upon publication due to legal restrictions preventing unrestricted public distribution. The data that support the findings of this study are available upon reasonable request from the authors.

Acknowledgment

The authors want to thank the technical stuff at CNAO for their support when running experiments. Anestis Nakas would like to express thanks for the support of the European Union's Horizon 2020 research and innovation program under the Marie Skłodowska-Curie Grant RAPTOR—Real-Time Adaptive Particle Therapy of Cancer, Grant Agreement No. 955956.

Author contributions

Conceptualization, T S and A N; software, T S, A N, C G, L V, M Do; data analysis, T S; image data acquisition, A V, V V, M C; experimental data acquisition, T S, A N, MC M, C G, writing—original draft preparation, T S, A N; visualization, TS; supervision CP, M Du, C G, G B; project administration, M Du, C G; funding acquisition, M Du, G B, All authors have read and agreed to the published version of the manuscript.

Institutional review board statement

The study was conducted in accordance with the Declaration of Helsinki, and approved by the Institutional Review Board (or Ethics Committee) of CENTRO NAZIONALE DI ADROTERAPIA ONCOLOGICA (CNAO) (protocol code CNAO 37-2019 4D-MRI, 2019).

Informed consent statement

Informed consent was obtained from all subjects involved in the study.

Conflict of interest

The authors declare no conflict of interest. Timo Steinsberger is now working for Brainlab AG, Olof-Palme-Straße 9, Munich, Germany without any conflict of interest.

Appendix

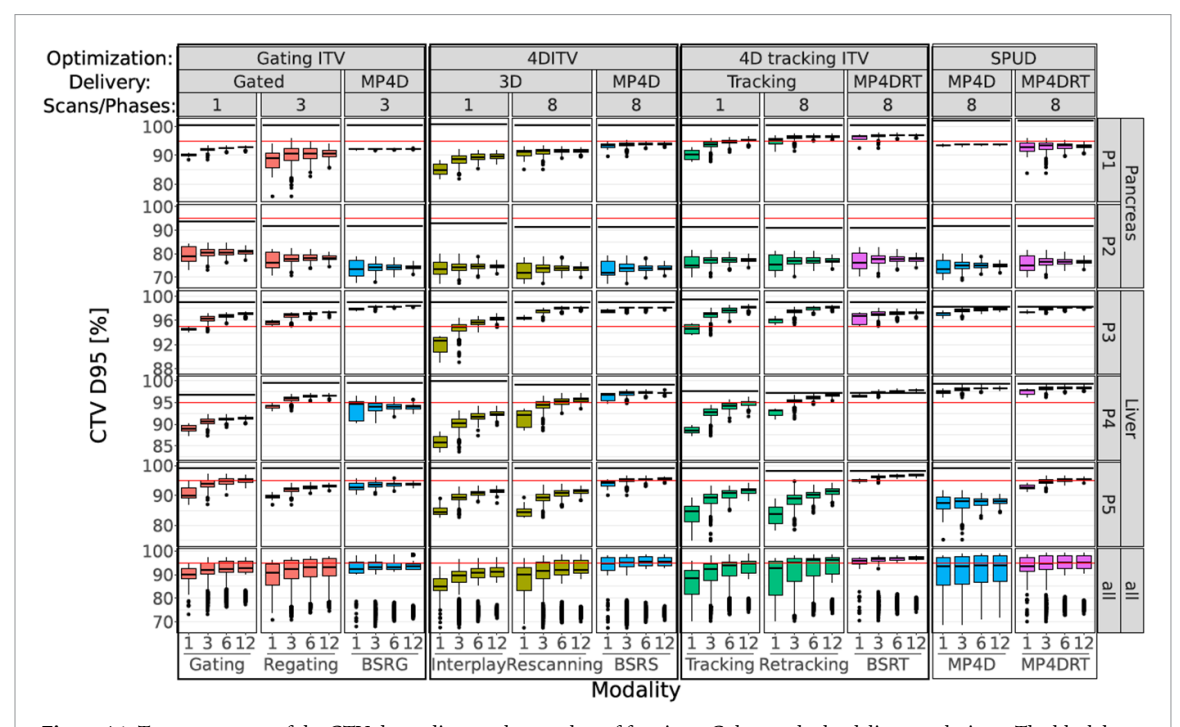
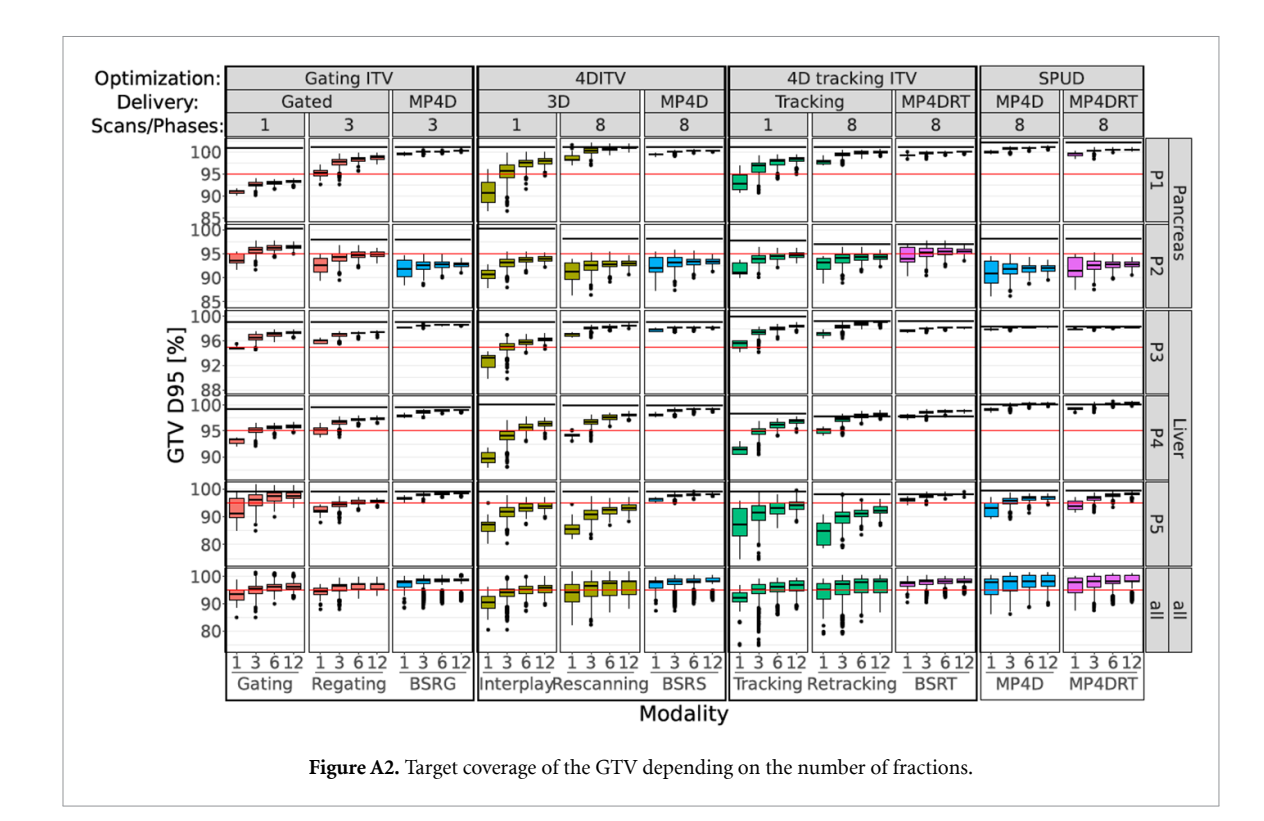
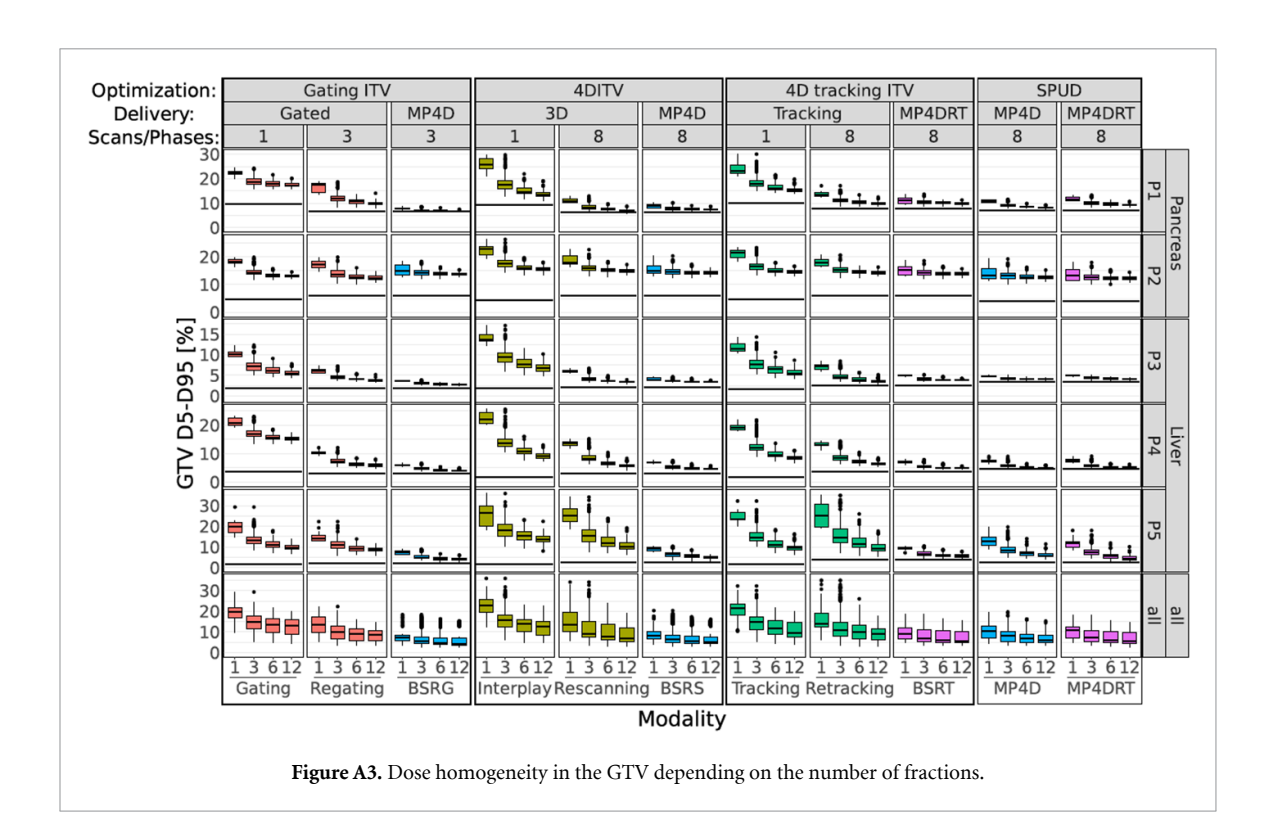


Figure A1. Target coverage of the CTV depending on the number of fractions. Colors code the delivery technique. The black bar represents the value from the planned dose distribution, the red line is the 95% acceptance criterion.





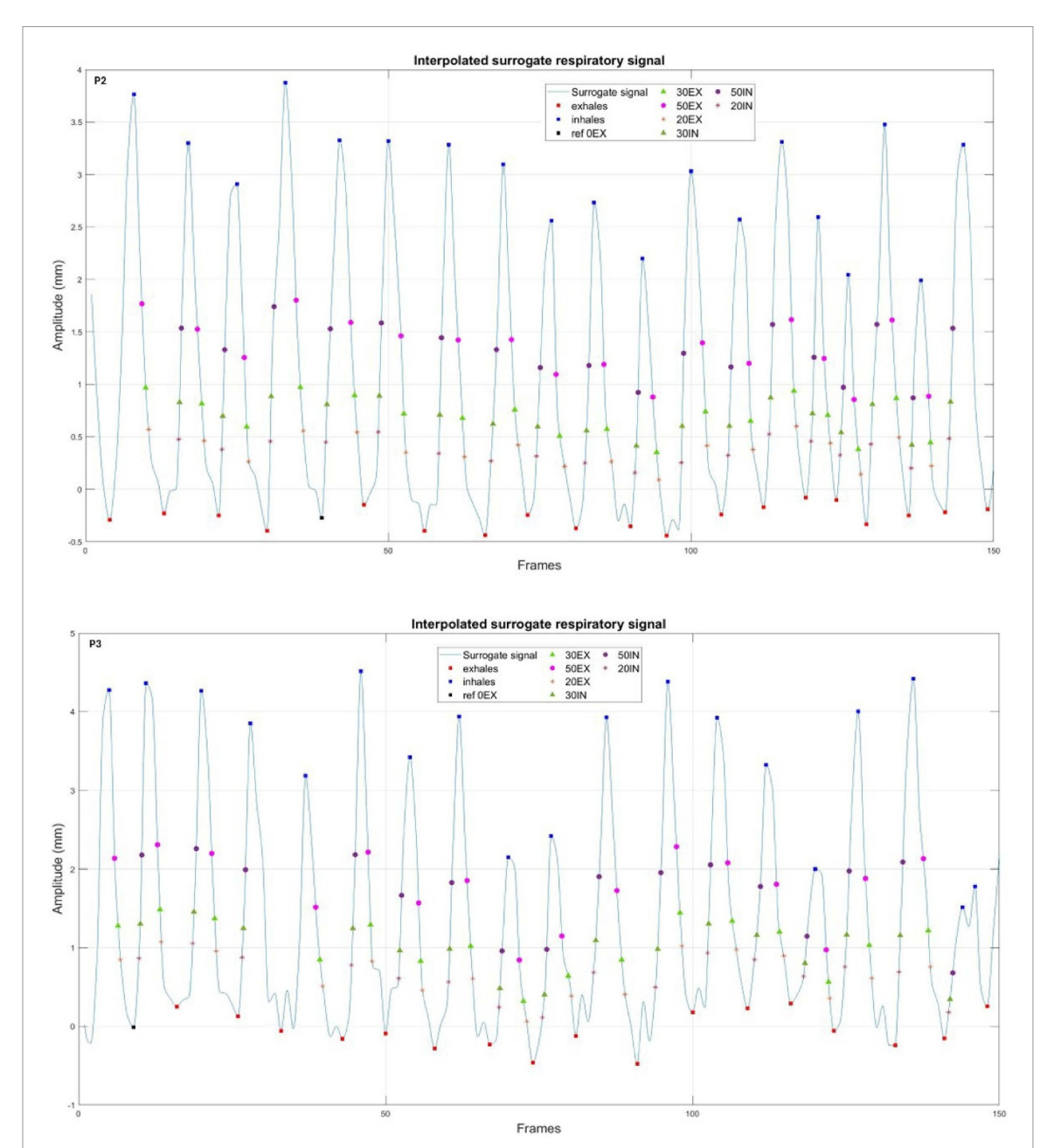


Figure A4. 1D surrogate respiratory signals extracted from the cine-MRI frames of patients P2–P3, by deformably registering cine-MRI frames on a reference end-exhale frame (ref 0EX).

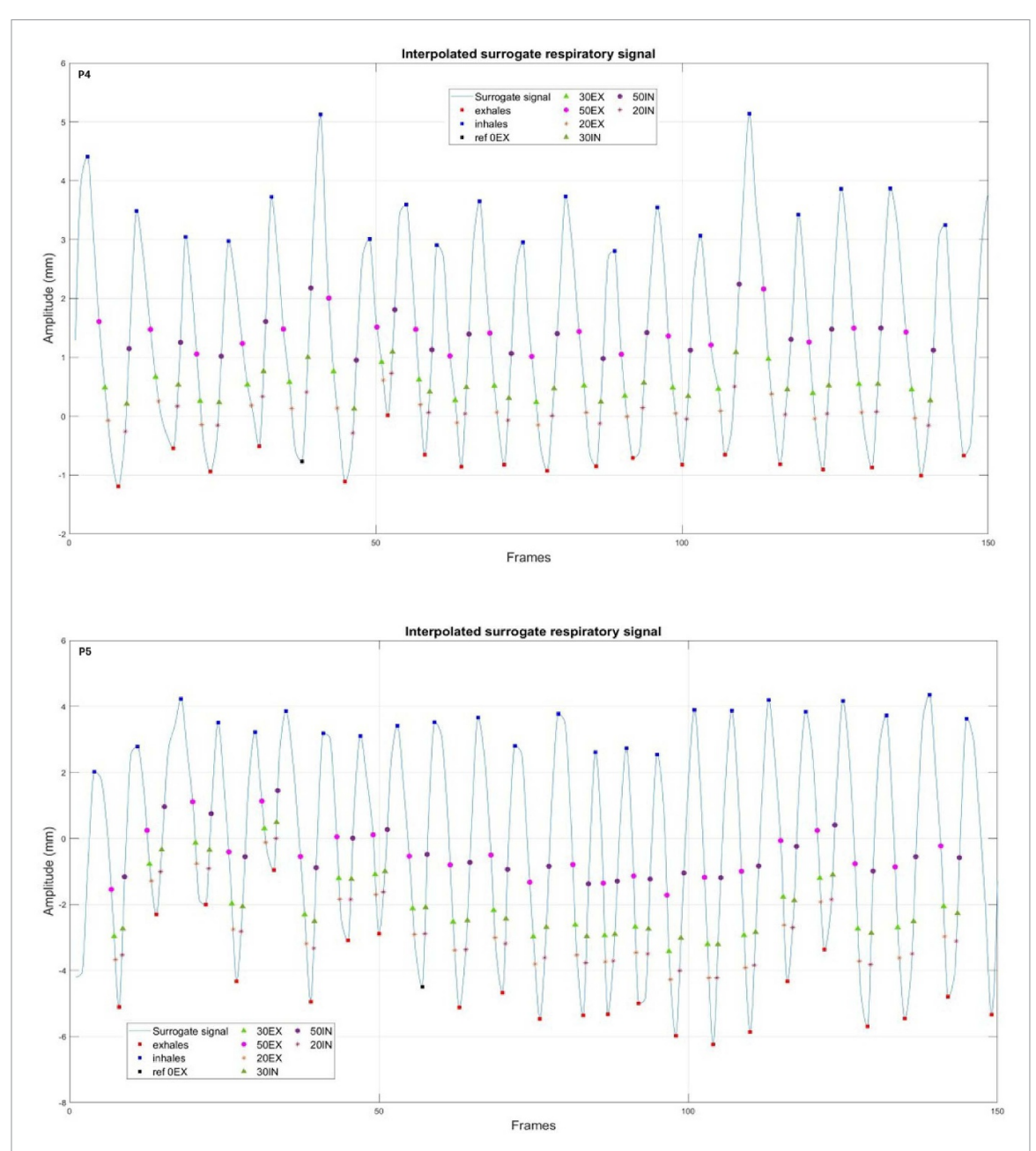


Figure A5. 1D surrogate respiratory signals extracted from the cine-MRI frames of patients P4–P5, by deformably registering cine-MRI frames on a reference end-exhale frame (ref 0EX).

ORCID iDs

Anestis Nakas © https://orcid.org/0009-0000-2813-0972

Marco Donetti © https://orcid.org/0000-0001-7489-6274

Maria Chiara Martire © https://orcid.org/0009-0006-5331-9463

Cosimo Galeone © https://orcid.org/0009-0006-4048-1728

Amelia Barcellini © https://orcid.org/0000-0002-1595-104X

Lennart Volz © https://orcid.org/0000-0003-0441-4350

Marco Durante © https://orcid.org/0000-0002-4615-553X

Christian Graeff © https://orcid.org/0000-0002-5296-7649

References

Batista V, Richter D, Combs S E and Jäkel O 2017 Planning strategies for inter-fractional robustness in pancreatic patients treated with scanned carbon therapy *Radiat. Oncol.* 12 1–9

Bert C and Durante M 2011 Motion in radiotherapy: particle therapy Phys. Med. Biol. 56 R113

- Dhont J et al 2018 The long- and short-term variability of breathing induced tumor motion in lung and liver over the course of a radiotherapy treatment Radiother. Oncol. 126 339–46
- Donetti M, Giordanengo S, Graeff C, Lis M, Milian F M, Pullia M, Steinsberger T, Vignati A and Rossi S 2021 Current and future technologies of the CNAO dose delivery system *IEEE Instrum. Meas. Mag.* 24 61–69
- Duetschler A et al 2022 Synthetic 4DCT(MRI) lung phantom generation for 4D radiotherapy and image guidance investigations Med. Phys. 49 2890–903
- Durante M and Loeffler J S 2010 Charged particles in radiation oncology Nat. Rev. Clin. Oncol. 7 37-43
- Furukawa T, Inaniwa T, Sato S, Tomitani T, Minohara S, Noda K and Kanai T 2007 Design study of a raster scanning system for moving target irradiation in heavy-ion radiotherapy *Med. Phys.* 34 1085–97
- Garau N, Via R, Meschini G, Lee D, Keall P, Riboldi M, Baroni G and Paganelli C 2019 A ROI-based global motion model established on 4DCT and 2D cine-MRI data for MRI-guidance in radiation therapy *Phys. Med. Biol.* 64 045002
- Graeff C 2014 Motion mitigation in scanned ion beam therapy through 4D-optimization Phys. Med. 30 570-7
- Hamaide V, Souris K, Dasnoy D, Glineur F and Macq B 2023 Real-time image-guided treatment of mobile tumors in proton therapy by a library of treatment plans: a simulation study *Med. Phys.* **50** 465–79
- Harris W, Ren L, Cai J, Zhang Y, Chang Z and Yin F F 2016 A technique for generating volumetric cine-magnetic resonance imaging Int. J. Radiat. Oncol. Biol. Phys. 95 844–53
- Kalantzopoulos C, Meschini G, Paganelli C, Fontana G, Vai A, Preda L, Vitolo V, Valvo F and Baroni G 2020 Organ motion quantification and margins evaluation in carbon ion therapy of abdominal lesions *Phys. Med.* 75 33–39
- Kanai T, Paz A, Furuichi W, Liu C S, He P and Mori S 2020 Four-dimensional carbon-ion pencil beam treatment planning comparison between robust optimization and range-adapted internal target volume for respiratory-gated liver and lung treatment *Phys. Med.* 80 277–87
- Lebbink F, Stock M, Georg D and Knäusl B 2022 The influence of motion on the delivery accuracy when comparing actively scanned carbon ions versus protons at a synchrotron-based radiotherapy facility *Cancers* 14 1788
- Lis M, Donetti M, Newhauser W, Durante M, Dey J, Weber U, Wolf M, Steinsberger T and Graeff C 2020 A modular dose delivery system for treating moving targets with scanned ion beams: performance and safety characteristics, and preliminary tests *Phys. Med.* 76 307–16
- Meijers A, Knopf A C, Crijns A P, Ubbels J F, Niezink A G, Langendijk J A, Wijsman R and Both S 2020 Evaluation of interplay and organ motion effects by means of 4D dose reconstruction and accumulation *Radiother. Oncol.* 150 268–74
- Meschini G et al 2022a Time-resolved MRI for off-line treatment robustness evaluation in carbon-ion radiotherapy of pancreatic cancer Med. Phys. 49 2386–95
- Meschini G *et al* 2022b Investigating the use of virtual 4DCT from 4DMRI in gated carbon ion radiation therapy of abdominal tumors *Z. Biomed. Phys.* 32 98–108
- Meschini G, Paganelli C, Gianoli C, Summers P, Bellomi M, Baroni G and Riboldi M 2019 A clustering approach to 4D MRI retrospective sorting for the investigation of different surrogates *Phys. Med.* 58 107–13
- Mori S and Furukawa T 2016 Rapid phase-correlated rescanning irradiation improves treatment time in carbon-ion scanning beam treatment under irregular breathing *Phys. Med. Biol.* 61 3857
- Paganelli C et al 2018a MRI-guidance for motion management in external beam radiotherapy: current status and future challenges Phys. Med. Biol. 63 22TR03
- Paganelli C, Lee D, Kipritidis J, Whelan B, Greer P B, Baroni G, Riboldi M and Keall P 2018b Feasibility study on 3D image reconstruction from 2D orthogonal cine-MRI for MRI-guided radiotherapy *J. Med. Imaging Radiat. Oncol.* 62 389–400
- Poulsen P R, Eley J, Langner U, Simone C B and Langen K 2018 Efficient interplay effect mitigation for proton pencil beam scanning by spot-adapted layered repainting evenly spread out over the full breathing cycle Int. J. Radiat. Oncol. Biol. Phys. 100 226–34
- Segars W P, Mahesh M, Beck T J, Frey E C and Tsui B M 2008 Realistic CT simulation using the 4D XCAT phantom *Med. Phys.* 35 3800–8 Steinsberger T P 2022 Development and experimental validation of adaptive conformal particle therapy *PhD Thesis* Technische Universität Darmstadt (https://doi.org/10.26083/tuprints-00021769)
- Steinsberger T, Alliger C, Donetti M, Krämer M, Lis M, Paz A, Wolf M and Graeff C 2021 Extension of RBE-weighted 4D particle dose calculation for non-periodic motion *Phys. Med.* **91** 62–72
- Steinsberger T, Donetti M, Lis M, Volz L, Wolf M, Durante M and Graeff C 2023 Experimental validation of a real-time adaptive 4D-optimized particle radiotherapy approach to treat irregularly moving tumors *Int. J. Radiat. Oncol.* Biol.* Phys.* 115 1257–68
- Stemkens B, Tijssen R H, Senneville B D D, Lagendijk J J and Berg C A V D 2016 Image-driven, model-based 3D abdominal motion estimation for MR-guided radiotherapy *Phys. Med. Biol.* **61** 5335–55
- Takao S, Miyamoto N, Matsuura T, Onimaru R, Katoh N, Inoue T, Sutherland K L, Suzuki R, Shirato H and Shimizu S 2016 Intrafractional baseline shift or drift of lung tumor motion during gated radiation therapy with a real-time tumor-tracking system a preliminary version of this study was presented at the 55th Annual Meeting of the American Society for Radiation Oncology Int. J. Radiat. Oncol. Biol. Phys. 94 172–80
- Wolf M, Anderle K, Durante M and Graeff C 2020 Robust treatment planning with 4D intensity modulated carbon ion therapy for multiple targets in stage IV non-small cell lung cancer *Phys. Med. Biol.* 65 215012
- Zhang Y et al 2023 A survey of practice patterns for real-time intrafractional motion-management in particle therapy Phys. Imaging Radiat. Oncol. 26 100439
- Zhang Y, Knopf A C, Weber D C and Lomax A J 2015 Improving 4D plan quality for PBS-based liver tumour treatments by combining online image guided beam gating with rescanning *Phys. Med. Biol.* 60 8141
- Zhou Y, Sakai M, Li Y, Kubota Y, Okamoto M, Shiba S, Okazaki S, Matsui T and Ohno T 2023 Robust beam selection based on water equivalent thickness analysis in passive scattering carbon-ion radiotherapy for pancreatic cancer *Cancers* 15 2520